Value-Based Noise Reduction for Low-Dose Dual-Energy Computed Tomography

Michael Balda[1], Björn Heismann[1,2], and Joachim Hornegger[1]

[1] Pattern Recognition Lab, Friedrich-Alexander University, Erlangen, Germany
[2] Siemens Healthcare, Erlangen, Germany

Abstract. We introduce a value-based noise reduction method for Dual-Energy CT applications. It is based on joint intensity statistics estimated from high- and low-energy CT scans of the identical anatomy in order to reduce the noise level in both scans. For a given pair of measurement values, a local gradient ascension algorithm in the probability space is used to provide a noise reduced estimate. As a consequence, two noise reduced images are obtained. It was evaluated with synthetic data in terms of quantitative accuracy and contrast to noise ratio (CNR)-gain. The introduced method allows for reducing patient dose by at least 30% while maintaining the original CNR level. Additionally, the dose reduction potential was shown with a radiological evaluation on real patient data. The method can be combined with state-of-the-art filter-based noise reduction techniques, and makes low-dose Dual-Energy CT possible for the full spectrum of quantitative CT applications.

1 Introduction

Dual-Energy CT (DECT) measures two image-sets at different energy weightings, e.g. by performing two scans with tube voltages set to 80kV and 140kV respectively. Alvarez [1] and Macovski [2] introduced a reconstruction technique for multi-energy scans based on a decomposition of the spectral attenuation coefficient into basis functions. Dual-Energy applications can yield valuable information for intervention planning and diagnosis. The most popular current Dual-Energy CT diagnostic applications are bone removal [3], PET/SPECT attenuation correction [4], lung perfusion diagnostic or quantification of contrast agent concentrations, for instance in the myocardium.

It is commonly agreed that the two dual-energy scans should require about the same total X-ray dose as the corresponding single-energy scan. This calls for effective noise reduction techniques in Dual-Energy CT. The most common filtering strategy applied in medical CT scanners is modifying the high-pass reconstruction kernel used for filtered back-projection (FBP) in a way that high frequencies are less amplified or blocked. Additionally, adaptive filters are applied occasionally. This type of filters steers the filter strength according to a noise estimate. It causes less smoothing in regions where noise is low, i.e. the X-rays are weakly attenuated. More sophisticated edge preserving filters have also been investigated. Weickert [5] introduced an edge-preserving anisotropic diffusion

T. Jiang et al. (Eds.): MICCAI 2010, Part III, LNCS 6363, pp. 547–554, 2010.

filter which can be adapted to CT data as shown in [6]. Bilateral filtering [7] tries to achieve a similar goal by combining frequency- and intensity-based smoothing. These filters steer the smoothing locally according to distance and similarity of neighboring intensity values. In CT, frequency based noise reduction filters are usually applied in the projection domain as the spectral noise properties in the CT-image or -volume domain can hardly be derived analytically. The image noise is inhomogeneous and non-stationary and estimating local noise properties is complex, [8] shows how to estimate local variance and analyze noise correlations for filtering CT-data in the image domain.

We introduce a noise reduction technique that is solely based on joint intensity statistics of the two Dual-Energy datasets. Most multi-energy modalities have an unequal noise distribution between images due to tube limitations and/or strong absorption in low-kVp images. The individual images from a multi-energy scan are much noisier than an image of a single energy scan, as the overall scan dose should be in an identical range. Quantitative CT (QCT) applications based on dual energy data are very sensitive to image noise. Image-based basis material decomposition (BMD) [9], for instance, causes noise amplification in the resulting basis material coefficient images. For other QCT applications, like Rho-Z projection [10], similar problems arise.

The proposed Dual-Energy noise reduction improves images from one energy weighting by using knowledge on the joint intensities from both datasets. As it is purely value-based and does not utilize any frequency information, it is compatible with the frequency-based filters explained above. This method operates on the reconstructed images, so it can be applied to any reconstructed DECT data-set. Since it is a post-reconstruction method, it may not enhance the quantitative correctness of the reconstructed images and relies on the correctness of the DECT reconstruction and beam hardening correction method.

2 Method

As input data, the noise-reduction method uses a low-kVp CT-volume $\bar{\mu}_1(\mathbf{x})$ and a high-kVp volume $\bar{\mu}_2(\mathbf{x})$. The voxel coordinate is indicated by $\mathbf{x}$. This method is neither restricted in terms of the number of multi-energy input datasets nor their dimension. However, for practical reasons, the description focuses on Dual-Energy data of two or three spatial dimensions. Our method estimates the most likely true object attenuation values $\widetilde{\mu}_1(\mathbf{x})$ and $\widetilde{\mu}_2(\mathbf{x})$ for each measured $(\bar{\mu}_1(\mathbf{x}), \bar{\mu}_2(\mathbf{x}))$-pair by a gradient ascent in the joint histogram.

Joint histogram computation: The first step is estimating the joint probability density $P(\bar{\mu_1}, \bar{\mu_2})$ for all $(\bar{\mu}_1(\mathbf{x}), \bar{\mu}_2(\mathbf{x}))$-pairs. Several methods are available for this purpose, e.g. computing histograms, data clustering or Parzen windowing [11]. We use kernel density estimation using a bivariate, uncorrelated Normal Distribution as kernel function. This method offers the possibility to apply smoothing to the $P(\bar{\mu}_1, \bar{\mu}_2)$-estimate by adjusting the bandwidth of the kernel:

$$\mathcal{N}_{(\sigma_1,\sigma_2)}(\bar{\mu}_1, \bar{\mu}_2) = \frac{1}{2\pi\sigma_1\sigma_2} \exp\left\{-\frac{1}{2}\left(\frac{\bar{\mu}_1^2}{\sigma_1^2} + \frac{\bar{\mu}_2^2}{\sigma_2^2}\right)\right\}. \quad (1)$$

The standard deviation (σ_1, σ_2) is the bandwidth parameter. Slightly oversmoothed density estimates yield better noise suppression at the cost of increased bias. In the following, the selected bandwidth parameter set is denoted (b_1, b_2). Once a set of bandwidth parameters is selected, the density estimate $P_{b_1,b_2}(\bar{\mu}_1, \bar{\mu}_2)$ can be computed by a convolution.

Noise estimation: The next step is to estimate true attenuation values for each pair of measured values by analyzing $P_{b_1,b_2}(\bar{\mu}_1, \bar{\mu}_2)$. In order to find the most probable true $\bar{\mu}_1$-value for $(\bar{\mu}_1(\mathbf{x}), \bar{\mu}_2(\mathbf{x}))$, the $\bar{\mu}_2(\mathbf{x})$-value is kept fixed and a gradient ascent along the $\bar{\mu_1}$-direction within the density estimate is performed.

The gradient direction is given by

$$G_1(\bar{\mu_1}, \bar{\mu_2}) = \left(\operatorname{sgn} \left\{ \frac{\mathrm{d}}{\mathrm{d}\bar{\mu}_1} \left(P_{(b_1,b_2)}(\bar{\mu}_1, \bar{\mu}_2) \right) \right\}, 0 \right). \tag{2}$$

Figure 1 shows an example for this procedure. The resulting local maximum for $\bar{\mu}_1(\mathbf{x})$ is called $\widetilde{\mu}_1(\mathbf{x})$. It represents the most probable $\bar{\mu}_1$-value for the measured intensity pair with fixed $\bar{\mu}_1(\mathbf{x})$. The distance $d_1(\mathbf{x}) = |\widetilde{\mu}_1(\mathbf{x}) - \bar{\mu}_1(\mathbf{x})|$ is an estimate for the noisiness of $\bar{\mu}_1(\mathbf{x})$. If the actually measured value $\bar{\mu}_1(\mathbf{x})$ is very close to the most probable value, it is likely to be less noisy. The process of finding the $\widetilde{\mu}_2$-value works analogously: The gradient ascent is performed in $\bar{\mu}_2$-direction. This leads to the estimates $\widetilde{\mu}_2(\mathbf{x})$ and $d_2(\mathbf{x})$.

Parameter reduction: The method has two bandwidth parameters of the bivariate Gaussians. These can be reduced to b_1 as the only free parameter and automatically compute an appropriate b_2 value for the $\bar{\mu}_2$-image by taking the relative contrast and noise of the $\bar{\mu}_2$-image into account:

We generate a set $\mathcal{X}$ of all soft tissue voxel positions in image 1 by thresholding. The standard deviations $\sigma_{1,\mathcal{X}}$ and $\sigma_{2,\mathcal{X}}$ are computed for $\mathcal{X}$ in both images. The standard deviation for the second image $\sigma_{2,\mathcal{X}}$ can differ from $\sigma_{1,\mathcal{X}}$ for two reasons: A different noise level and/or a different tissue contrast in the second image. A lower noise level or less contrast require a smaller bandwidth. A higher bandwidth can be chosen if the noise level lower or the tissue contrast is higher. Consequently we set $b_2 = b_1 \cdot \frac{\sigma_{2,\mathcal{X}}}{\sigma_{1,\mathcal{X}}}$. For the example of a second image with a higher tube acceleration voltage at the same tube current, a lower noise level and reduced tissue contrast is observed. This case leads to a reduced bandwidth b_2. If the noise level is similar in both images, the reduced tissue contrast prohibits strong noise reduction on the high-kVp image.

Noise reduction: The quality of the estimates $\widetilde{\mu}_1(\mathbf{x})$ and $\widetilde{\mu}_2(\mathbf{x})$ is affected by noise in the original intensity pairs $(\bar{\mu_1}(\mathbf{x}), \bar{\mu_2}(\mathbf{x}))$: High noise in $\bar{\mu}_1(\mathbf{x})$ and $\bar{\mu}_2(\mathbf{x})$ generally worsens both estimates, low noise in the $\bar{\mu}_1(\mathbf{x})$-value increases the quality of the estimate $\widetilde{\mu}_2(\mathbf{x})$ and vice versa. The noise-reduction process should use a measure that takes these properties into account and adjusts the strength of the correction process accordingly. The following measure offers these properties and allows governing the strength of the filter by a single parameter:

$$\widehat{\mu}_1(\mathbf{x}) = \alpha(\mathbf{x}) \cdot \bar{\mu}_1(\mathbf{x}) + (1 - \alpha(\mathbf{x})) \cdot \widetilde{\mu}_1(\mathbf{x}) \tag{3}$$

The correction strength is defined by a parameter α, the final noise-reduced image value is called $\widehat{\mu}_1(\mathbf{x})$; α is computed as follows:

$$\alpha(\mathbf{x}) = \left(\frac{d_1(\mathbf{x})}{d_t(\mathbf{x})}\right)^r \text{ with } d_t(\mathbf{x}) = \sqrt{d_1(\mathbf{x})^2 + d_2(\mathbf{x})^2} \tag{4}$$

The parameter r determines the correction strength, values of $r = [0, 1]$ generally favor the $\widetilde{\mu}_1(\mathbf{x})$- resp. $\widetilde{\mu}_2(\mathbf{x})$-estimates whereas $r =]1, +\infty[$ directs the filter to use the estimates only when the image noise estimate is close to the overall noise estimate $d_t(\mathbf{x})$. In our experiments, we used $r = 5$.

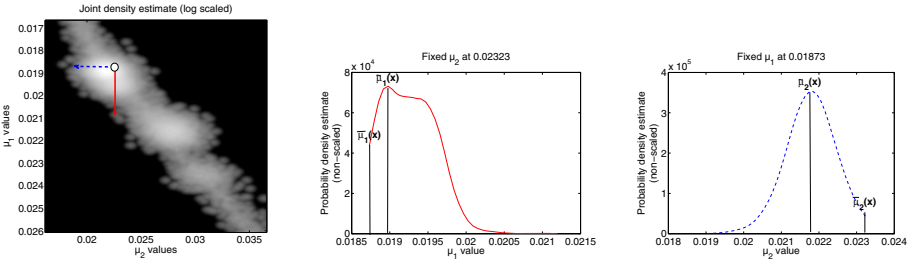

(a) PDF-estimate for large bandwidth

(b) Line plot for $\tilde{\mu}_1(\mathbf{x})$ estimation.

(c) Line plot for $\tilde{\mu}_2(\mathbf{x})$ estimation.

Fig. 1. Examples for the gradient ascent procedure with $\mu_1(\mathbf{x}) = 0.0187\,\mathrm{mm}^{-1}$ and $\mu_2(\mathbf{x}) = 0.0232\,\mathrm{mm}^{-1}$. Arrows indicate the gradient direction, the start point is located at the base of the arrows.

3 Evaluation

In order to evaluate the theoretical limits of the proposed denoising method against ground truth data, we conducted several simulations and a radiological evaluation.

1. *Contrast-to-noise ratio*: Evaluation of the achievable CNR-gain for various contrasts and dose-levels.
2. *Quantitative accuracy and precision*: Noise reduction and quantitative accuracy for energy calibration application using basis material decomposition.
3. *Radiological evaluation*: Perceived and measured noise reduction while maintaining visibility of important image details.

The simulations involve an analytic forward projection of a geometrically defined thorax phantom and a standard filtered back-projection (see Fig. 2). The tissue compositions were taken from the ICRU Report 46[1] and the elemental mass attenuation coefficients from [12]. In order to avoid beam hardening artifacts, we created dual-energy data-sets with mono-chromatic radiation at 54 keV and 73 keV which corresponds to the effective energy of 80 kVp and 140 kVp scans.

[1] International Commission on Radiation Units and Measurements: Report 46. Photon, Electron, Proton and Neutron Interaction Data for Body Tissues, 1998.

(a) (b) (c)

Fig. 2. (a) Thorax phantom (with a small water cylinder at the top-left corner used for water scaling); (b) Low contrast lesions for CNR evaluation. (c) Lesion example at 80 kVp with 14 HU contrast and 70000 primary photons (intensity window center: 45 HU, width: 35 HU).

Contrast-to-noise ratio: The possible improvement in contrast-to-noise ratio (CNR) of the data was evaluated by placing various small lesions inside the liver (see Fig. 2b). Four different contrasts of where evaluated at five noise levels. The liver and cirrhotic liver tissue composition was chosen according to the ICRU report 46 with a density of $1.060\frac{\mathrm{g}}{\mathrm{cm}^3}$ for the healthy liver tissue. The liver lesion densities were set to $1.040, 1.045, 1.050$ and $1.055\frac{\mathrm{g}}{\mathrm{cm}^3}$. The resulting contrasts are $29, 24, 19$ and 14 HU for the effective 80 kV spectrum and $23, 18, 13$ and 8 HU for the 140 kV spectrum. The ratio of quanta in the low and high energy spectra was kept fix at 3 to 1. Six different bandwidths were selected for the parameter b_1: $0.5, 1.0, 2.0, 4.0, 7.0$ and 11.0 HU. The according b_2-values were determined automatically. Figure 3 shows an excerpt of the resulting CNR-values. The results show an improvement in all cases as long as an appropriate bandwidth parameter is chosen. The choice of a too large bandwidth can, however, decrease the resulting CNR for very low contrasts. The possible dose reduction can be deduced by comparing the number of primary photons needed to get a CNR value similar to the original one. In the evaluated cases, 70% to 40% of the original photon numbers yield similar CNR values. In general, the CNR gain is larger in the 140 kV cases, since the tissue contrast in the 140 kV images is smaller, so even small improvements with respect to noise have a large impact in terms of CNR.

Quantitative accuracy and precision: For this evaluation we performed a two-material BMD with the basis materials water and femur bone on the thorax phantom introduced above. The liver lesions were removed and the medium noise case was selected with $1.4 \cdot 10^5$ primary photons for the effective 80 kVp spectrum. Here we use the BMD to estimate the spectral attenuation coefficients $\mu(E, \mathbf{x})$ at every voxel position $\mathbf{x}$. These coefficients are then weighted with an effective 120 kVp spectrum ($w_{120\,\mathrm{kVp}}(E)$) to create a virtual 120 kVp image from the input images by computing $\bar{\mu}_{120\mathrm{kVp}}(\mathbf{x}) = \int_0^\infty w_{120\,\mathrm{kVp}}(E)\mu(E, \mathbf{x})dE$. The resulting image is compared with the analytically computed ground truth data in terms of mean-shift and standard deviation. The value-based noise reduction may cause a minor shift of the mean attenuation values along with noise reduction. This evaluation is meant to quantify the trade-off between noise reduction and decrease in quantitative accuracy caused by the mean shift.

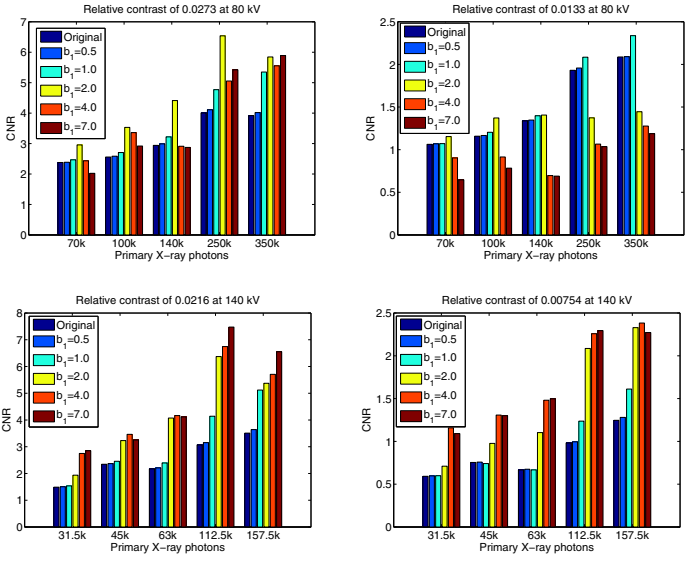

Fig. 3. CNR test results for different contrasts at 80 kVp and 140 kVp tube voltage and selected noise reduction parameters.

Table 1. Ground truth and calculated mean and standard deviation of attenuation values for virtual 120 kVp image from original and processed images. All quantities given in mm^{-1}. The values show a very small bandwidth dependence of the quantitative accuracy (mean values). The noise (standard deviation) decreases with increasing bandwidth.

Bandwidth	Average soft tissue	Healthy liver	Red Marrow
Ground Truth	2.072e-2	2.156e-2	2.050e-2
Original	2.060e-2 (1.605e-4)	2.140e-2 (1.655e-4)	2.039e-2 (3.711e-4)
1.08e-5	2.060e-2 (1.583e-4)	2.140e-2 (1.647e-4)	2.040e-2 (3.714e-4)
4.33e-5	2.059e-2 (1.286e-4)	2.140e-2 (1.526e-4)	2.044e-2 (3.643e-4)
8.66e-5	2.058e-2 (0.859e-4)	2.139e-2 (1.001e-4)	2.051e-2 (3.204e-4)
1.52e-4	2.059e-2 (1.002e-4)	2.138e-2 (1.094e-4)	2.054e-2 (2.665e-4)

Table 1 shows the results at different bandwidths for the tissues average soft tissue (large area), liver (medium area) and red marrow (small area). Noise suppression is achieved for all tissues at a tolerable mean shift. At lower bandwidths the mean shift is almost negligible. At very high bandwidths the noise standard deviation can get worse in some cases since the gradient ascent tends to the wrong direction for some voxels.

Radiological evaluation: Images from seven different Dual-Energy scans were presented to three radiologists in a typical clinical environment. We selected data from typical examinations of different body regions with and without contrast agents and varying scan parameters. The input images were all Dual-Source

images acquired with a Siemens Definition or a Siemens Definition Flash CT-scanner (Siemens AG, Forchheim, Germany). The Siemens Definition device uses 80 kVp and 140 kVp tube voltages, whereas the Definition Flash uses 100 kVp and 140 kV with an additional tin-filter for the high-energy spectrum that improves spectral separation. The images were presented in randomly ordered pairs of original and denoised images with different bandwidth settings. The radiologists were asked to compare the image-pairs in terms of perceived noise level and visibility of important details. We evaluate to which extent the perceived and measured noise level can be reduced without important structures being visibly weakened compared to the original images. The corresponding bandwidth parameter for each dataset is called *optimal bandwidth* in the following. Table 2 lists the average measured noise reduction for the optimal bandwidth on all datasets. All radiologists agreed that using the optimal bandwidth, a noise reduction could be perceived in all Dual-Energy datasets.

Table 2. Average noise reduction for several different test scenarios with optimal bandwidth setting. First number corresponds to low-kVp image, second to high-kVp. Image noise was determined by evaluating the standard deviation in homogeneous image regions. (*) only 80kV image was evaluated for the "Foot" dataset.

Dataset	Head	Foot*	Liver	Lung
Noise reduction	−27%/ − 25%	−33%*	−29%/ − 25%	−29%/ − 25%
	Abdomen	Lower Abdomen	Pelvis	
	−20%/ − 32%	−24%/ − 18%	−22%/ − 22%	

4 Conclusion

The introduced noise-reduction technique for Dual-Energy CT data showed the potential of reducing image noise by about 20 to 30% in subjective tests on real CT-images of various body regions. The quantitative accuracy was evaluated in an energy calibration application on phantom data. It revealed a tolerable accuracy loss of approx. 1 to 2% which is in the range of the overall accuracy of a CT system. The noise standard deviation could be reduced by approx. 30% for this application. A CNR test for small, low-contrast lesions yielded a CNR-gain ranging from 10% to over 100% depending on noise level, tube voltage setting and tissue contrast. The CNR values of the original image could be reproduced with 30% up to 70% less primary photons needed. This is directly related to an accordingly reduced radiation dose.

References

1. Alvarez, R.E., Macovski, A.: Energy-selective Reconstructions in X-ray Computerized Tomography. Phys. Med. Biol. 21(5), 733–744 (1976)
2. Macovski, A., Alvarez, R.E., Chan, J.L.H., Stonestrom, J.P., Zatz, L.M.: Energy dependent reconstruction in X-ray computerized tomography. Comput. Biol. Med. 6(4), 325–334 (1976)

3. Zheng, L., Maksimov, D., Stutzmann, T., Jochum, S., Brockmann, C., Diehl, S., Hesser, J.: Removal of bone information in dual energy CT. In: Proceedings of the MICCAI-CVII Workshop, pp. 120–127 (2008)
4. Heismann, B.J., Balda, M.: Quantitative image-based spectral reconstruction for computed tomography. Medical Physics 36(10), 4471–4485 (2009)
5. Weickert, J.: Anisotropic Diffusion in Image Processing. Teubner-Verlag, Stuttgart (1998)
6. Wang, J., Lu, H., Li, T., Liang, Z.: Sinogram noise reduction for low-dose CT by statistics-based nonlinear filters, vol. 5747, pp. 2058–2066. SPIE, San Jose (2005)
7. Tomasi, C., Manduchi, R.: Bilateral filtering for gray and color images. In: Sixth International Conference on Computer Vision (1998)
8. Borsdorf, A., Kappler, S., Raupach, R., Hornegger, J.: Analytic Noise Propagation for Anisotriopic Denoising of CT Images. In: Sellin, P. (ed.) 2008 IEEE Nuclear Science Symposium Conference Record, pp. 5335–5338 (2008)
9. Taguchi, K., Zhang, M., Frey, E.C., Xu, J., Segars, W.P., Tsui, B.M.W.: Image-domain material decomposition using photon-counting CT, vol. 6510, p. 651008. SPIE, San Jose (2007)
10. Heismann, B.J., Leppert, J., Stierstorfer, K.: Density and atomic number measurements with spectral X-ray attenuation method. J. Appl. Phys. 94(3), 2074–2079 (2003)
11. Parzen, E.: On estimation of a probability density function and mode. Ann. Math. Stat. 33, 1065–1076 (1962)
12. Berger, M.J., Hubbell, J.H., Seltzer, S.M., Chang, J., Coursey, J.S., Sukumar, R., Zucker, D.S.: XCOM: Photon Cross Sections Database. NIST Standard Reference Database 8 (XGAM) (1998)